Published in final edited form as:

Genesis. 2016 February ; 54(2): 91–98. doi:10.1002/dvg.22913.

Fgf3-Fgf4-cis: a new mouse line for studying *Fgf* functions during mouse development

Matthew J. Anderson[1], **Eileen Southon**[2], **Lino Tessarollo**[2], **Mark Lewandoski**[1,*]

[1]Cancer and Developmental Biology Laboratory, National Cancer Institute, Frederick, Maryland 21702

[2]Mouse Cancer Genetics Program, National Cancer Institute, Frederick, Maryland 21702

Abstract

The fibroblast growth factor (FGF) family consists of 22 ligands in mice and humans. FGF signaling is vital for embryogenesis and, when dysregulated, can cause disease. Loss-of-function genetic analysis in the mouse has been crucial for understanding FGF function. Such analysis has revealed that multiple *Fgfs* sometimes function redundantly. Exploring such redundancy between *Fgf3* and *Fgf4* is currently impossible because both genes are located on chromosome 7, about 18.5 kb apart, making the frequency of interallelic crossover between existing mutant alleles too infrequent to be practicable. Therefore, we retargeted *Fgf3* and *Fgf4* in cis, generating an *Fgf3* null allele and a conditional *Fgf4* allele, subject to Cre inactivation. To increase the frequency of cis targeting, we used an F1 embryonic stem cell line that contained 129/SvJae (129) and C57BL/6J (B6) chromosomes and targeting constructs isogenic to the 129 chromosome. We confirmed cis targeting by assaying for B6/129 allele-specific single-nucleotide polymorphisms. We demonstrated the utility of the $Fgf3^{\Delta}$-$Fgf4^{flox}$-cis mouse line by showing that the caudal axis extension defects found in the *Fgf3* mutants worsen when *Fgf4* is also inactivated. This $Fgf3^{\Delta}$-$Fgf4^{flox}$-cis line will be useful to study of redundancy of these genes in a variety of tissues and stages in development.

Keywords

FGF; FGF3; FGF4; Genetic redundancy; Mouse development; Presomitic Mesoderm; Axis extension

Results and Discussion

In humans and mice, fibroblast growth factor (FGF) signaling is controlled by a large family encoded by 22 ligand and 4 receptor genes (Ornitz and Itoh, 2015). FGF ligands are related by a core homology domain as well as secondary structure (Goetz and Mohammadi, 2013). They fall into three functional groups: the intracellular FGF homologous factors (FGFs 11-FGF14) that regulate voltage gated sodium channels (Goldfarb, 2005; Olsen et al., 2003), endocrine FGFs (FGF15/19, FGF21 and FGF 23) that regulate metabolic homeostasis (Itoh,

*Corresponding Author: National Cancer Institute, 1050 Boyles Street, Box B, Frederick, Maryland 21702, lewandom@mail.nih.gov, Telephone: (301) 846-5510, Fax: (301) 846-7117.

2010; Long and Kharitonenkov, 2011) and the largest group (FGF1-FGF10, FGF16-FGF18, FGF20, FGF22), the “canonical” or “paracrine” FGFs that play essential roles in nearly all tissues during embryogenesis and act to maintain homeostasis in the adult (Ornitz and Itoh, 2015).

Typically in a large gene family like the *Fgfs*, functional redundancy in some tissues occurs (Ornitz and Itoh, 2015). Uncovering such redundancy requires complex crosses to generate the appropriate genotype that lacks two or more genes. Such approaches are important, not only to address basic biological problems, but also to lay the foundation to effective treatment of disease states that can be complicated by redundant molecular signals, such as cancer (Sun and Bernards, 2014).

Functional redundancies between Fgfs have been previously described. For example, loss of function genetics reveals that *Fgf4* and *Fgf8* are functionally redundant during limb development (Boulet et al., 2004; Sun et al., 2002) and somitogenesis (Boulet and Capecchi, 2012; Naiche et al., 2011). *Fgf3* has been shown to act with *Fgf10* during cardiovascular development (Urness et al., 2011) and with *Fgf8* during pharyngeal segmentation (Jackson et al., 2014). However, we cannot determine what redundancy exists between *Fgf3* and *Fgf4* using current mutant mouse lines (Alvarez et al., 2003; Mansour et al., 1988; Moon et al., 2000; Sun et al., 2000) because these two genes lie in a head-to-tail arrangement on chomosome 7 with the *Fgf3* stop codon 18525 bp from the *Fgf4* start codon (Ensembl database). At this distance, the frequency of interallelic crossover of the existing mutant alleles for each gene is vanishingly small.

Therefore, we sought to produce a mouse line containing such a doubly targeted chromosome using gene targeting strategies in embryonic stem cells (ESCs). Although on some genetic backgrounds, a subset of *Fgf3* null homozygotes do not survive to weaning, a significant subset does survive and is viable and fertile (Hatch et al., 2007). *Fgf4* null homozygotes, however, do not advance beyond implantation (Feldman et al., 1995). Therefore we reasoned that generating mice with a targeted chromosome carrying an *Fgf3* null allele and an *Fgf4* allele flanked by LoxP sites (“floxed”), suitable for conditional Cre-mediated recombination, would be useful to explore redundancy between these two genes.

To increase the likelihood of targeting the loci in Cis, we used an ESC line that was derived from F1 progeny generated from a cross between 129/SvJae (129) and C57BL/6J (B6) mouse strains (You et al., 1998), and sought to use the propensity of constructs to recombine with isogenic DNA to favor gene targeting to the 129 chromosome in these cells. We first targeted the *Fgf4* locus using the exact construct we had previously used to successfully target this gene (Sun et al., 2000); this construct contains a FRT-flanked (“flrted”) neomycin-resistance cassette (Fig. 1a, right). Standard Southern mapping determined that 4/16 ESC clones contained the correctly targeted locus (Fig. 1b). We then used a PCR assay and determined all clones contained the “orphan” 3′ loxP site (Fig. 1c). Two such subclones were used to generate chimeric mice and one of these produced chimeras with an approximately 90% ESC contribution. Therefore we chose this subclone to retarget the *Fgf3* locus, replacing the entire coding region with a hygromyocin-resistance cassette (Fig. 1a, left). Southern mapping revealed *Fgf3* was correctly targeted at a frequency of 3/27.

We then used single-nucleotide polymorphisms (SNPs) between 129 and B6, as indicated in Figure 2a, to determine if we had targeted *Fgf3* and *Fgf4* in cis on the 129 chromosome in these final ESC subclones. We devised a strategy to produce PCR products containing the SNP-containing regions of each gene, which is disrupted in the targeted alleles (Fig. 2a). Therefore, since the only wildtype *Fgf4* PCR fragment we could amplify was B6 DNA, this indicated that we had targeted the 129 chromosome when we first targeted the ESC cells (Fig. 2a, b). Similarly, in 2 out of 3 clones targeted for *Fgf3*, we could only amplify a wildtype B6 PCR fragment, indicating the targeting event took place on the 129 chromosome. Thus in 2 out of 3 cases targeting took place in cis. Note that this SNP-based strategy is generally applicable to monitor *cis* or *trans* targeting whether one uses traditional homologous recombination techniques, as we have here, or CRISPR Cas9-based approaches (Yang et al., 2014), providing one starts with a hybrid F1 genome.

One of these cis-targeted ESC clones was used to generate a mouse line, using standard techniques (Reid and Tessarollo, 2009). We have bred this mouse line for more than 7 generations and separately PCR-genotyped for each targeted *Fgf* alleles and found that both *Fgf* loci are always inherited together, indicating our strategy to target these genes in *cis* was successful. We bred F1 cis-heterozygotes to βactin-Flpe mice (Rodriguez et al., 2000) to delete the flrted neomycin-resistance cassette within the *Fgf4* locus, because this cassette interferes with gene expression (Sun et al., 2000). Progeny of this cross that were heterozygous for $Fgf3^{\Delta}$-$Fgf4^{flox}$ (i.e. lacking the neomycin-resistance cassette) and positive for βactin-Flpe were crossed to NIH Swiss Webster mates to generate heterozygotes lacking βactin-Flpe. These mice were then intercrossed to generate homozygotes. However, of 49 progeny at weaning, only one homozygote was present. Of these 49, 15 were wildtype homozygotes for the *Fgf3-Fgf4* loci and approximately twice that were (33) were $Fgf3^{\Delta/wt}$-$Fgf4^{flox/wt}$-cis. Hence only the $Fgf3^{\Delta}$-$Fgf4^{flox}$ homozygotes were mostly missing. To explore this further, we examined progeny at E18.5 from an $Fgf3^{\Delta/wt}$-$Fgf4^{flox/wt}$-cis intercross that were a 129/B6/NIH Swiss Webster mix and found the homozygotes were underrepresented (Fig. 3a). We attributed this to the nullzygosity of *Fgf3,* because $Fgf4^{flox}$ homozygotes display no lethality and similar loss of *Fgf3* null homozygotes has been reported (Hatch et al., 2007; Mansour et al., 1993). We reasoned that the greater loss at weaning was due to competition with littermates during nursing because *Fgf3* null homozygotes are smaller than normal (Mansour et al., 1993). Indeed, we found that if we culled heterozygotes and wildtypes from early litters (identifiable because their tails are of normal length) from *Fgf3* null homozygotes (which have short tails) we soon had a large number of surviving homozygotes. We intercrossed these and established thriving colony of $Fgf3^{\Delta}$-$Fgf4^{flox}$ homozygotes.

Of three previously described *Fgf3* null mutants, two ($Fgf3^{tm1Mrc}$; MGI:1931059 and $Fgf3^{tm1.1Sms}$; MGI:3767558) resulted in incompletely penetrant inner ear defects that lead to circling or head-tilt behavior (Hatch et al., 2007; Mansour et al., 1993) and one ($Fgf3^{tm1Sng}$; MGI:3027990) did not have this phenotype (Alvarez et al., 2003). To determine if our new mutant allele displayed such behavior we examined $Fgf3^{\Delta}$-$Fgf4^{flox}$ homozygotes and found that 2 out of 19 displayed circling or head-tilting. Because there is no targeting feature common to the three alleles that display this aberrant behavior, it appears that background modifier(s) cause this *Fgf3*-specific defect. Consistent with this notion, when the $Fgf3^{tm1Sng}$

allele is bred into B6 background, a vestibular phenotype with these behaviors occurs with incomplete penetrance (T. Schimmang, personal comm.).

To test the utility of these mice for exploring redundancy in FGF signaling, we sought to inactivate *Fgf4* in the nascent mesoderm starting about embryonic day (E) 7.5, within an *Fgf3* null background. To achieve this, we performed the cross shown in Figure 3b. All progeny, including the genotype TCre; $Fgf3^{\Delta/\Delta}$-$Fgf4^{flox/\Delta}$ ("double mutants"), were found at nearly Mendelian ratios at E18.5. Therefore we speculate that a genetic modifier(s) affecting *Fgf3* viability that were present in our earlier crosses was lost from the colonies that produced the parents used in this experimental cross.

In double mutants, the axis truncation defects that occurs in *Fgf3* null homozygotes is significantly exacerbated (Fig. 3c–e). As E18.5 TCre;$Fgf4^{flox/\Delta}$ mutants have a normal tail length (data not shown) we conclude that these two genes act redundantly in caudal axis extension. We examined this redundant function at earlier stages by analyzing the size of the tailbud presomitic mesoderm (PSM) at E10.5, wherein lie the progenitors that will generate the axis that is affected in mutants in Figure 3c–e. To achieve this we assayed for the expression of both *Msgn1*, which marks the posterior PSM (Yoon and Wold, 2000) and *Uncx4.1,* which marks the posterior half of each somite (Mansouri et al., 2000) (Fig. 4a–d). The total PSM is the area between *Uncx4.1* expression in the caudal-most somite and the posterior limit of *Msgn1* expression (bracket in Fig. 4a). Furthermore, the *Msgn1* expression domain regresses as the posterior axis extends, eventually dwindling in the growing caudal axis and then disappearing as axis extension ceases (Gomez et al., 2008). The size of the *Msgn1* expression domain as well as the overall tailbud is reduced in *Fgf3* null homozygotes compared to littermate controls (Fig. 4c, e). There is an even greater reduction in double mutants (Fig. 4d, e), indicating genetic redundancy between these two *Fgfs* in maintenance of the PSM.

We anticipate that this new $Fgf3^{\Delta}$-$Fgf4^{flox}$-cis mouse line will be useful to explore FGF function in a variety of embryonic tissues and stages. Based on the coexpression domains of *Fgf3* and *Fgf4*, these tissues are the early implantation stages prior to gastrulation (Niswander and Martin, 1992), ear development (Wright et al., 2003), tooth development (Li et al., 2014), and pharyngeal pouch development (Hatch et al., 2007; Niswander and Martin, 1992; Urness et al., 2011; Wright et al., 2003). Furthermore, *Fgf3* is upregulated when both *Fgf4* and *Fgf8* are inactivated in the genital tubercle and limb bud AER, suggesting it may be redundantly functional with these two *Fgfs* in these tissues (Miyagawa et al., 2009). Therefore the $Fgf3^{\Delta}$-$Fgf4^{flox}$-cis mice may be useful to explore redundancy between *Fgf3*, *Fgf4* and *Fgf8*.

Methods and Materials

Ethics Statement

Mice were treated in accordance with the recommendations in the Guide for the Care and Use of Laboratory Animals (National Academies Press; 8th edition). The protocol was approved by the Animal Care and Usage Committee of NCI-Frederick (NIH) (Animal Study Proposal: 11-069).

Generation of Targeting Vectors

For targeting the *Fgf4* locus, we used the previously described targeting construct (Sun et al., 2000) to which we added a DTA cassette to the 3′ end. In targeting the *Fgf3* locus, we replaced the coding region, starting 261 bp upstream of the start codon and ending 1269 bp downstream of the stop codon (5810 bp total) with a hygromycin B selection-cassette. To construct the *Fgf3* targeting vector we generated a 4.2kb left homology arm through PCR amplification of 129 tail DNA and used a 3.1 kb right homology arm from a previously described targeting construct (Alvarez et al., 2003). Specifically, to generate the left homology arm we PCR-amplified a 2.2 kb fragment using primers with restriction sites (lower case) used for cloning: (5′-TAgcggccgcTAGATGACCTTGAACTCCTGGCTAG and 5′-CACAAATGAATCCAGAGGGCATCTGG) and 2.0 kb (5′-GCCAGGCACAGGAAGGTAAC and 5′-TActcgagGAGAGAGGTGGAGATGGAGATAAG) fragment from 129 tail DNA. An endogenous *BamH*I site at the 3′ end of the 2.2 kb product and at the 5′ end of the 2.0 kb product was used to cut the two fragments which were then ligated to form the 4.2 kb arm. Both of these arms were then ligated into a pBluescript vector (Stratagene) and a hygromycin B selection-cassette was added between the homology arms and a DTA cassette was added immediately 3′ to the right homology arm. Both targeting vectors were linearized by digestion with *Not*I prior to injection; *Not*I sites are present at the 5′ end of the left homology arms of each targeting construct.

Generation of Fgf3null-Fgf4flox-cis Mice

The *Fgf4flox*-targeting construct was first electroporated into a hybrid 129 Sv–C57Bl/6 ES cell line (You et al., 1998), as previously described (Tessarollo et al., 2009). Clones were screened by Southern blot analysis and PCR-screened as described in Figure 1 for insertion of the 3′ LoxP site (5′-TCTGGAGAGGAACTAGGAATGG and 5′-GAAGAGAAGCAGGCAGATGC). Two positive clones were tested for ability to contribute to chimeras in albino-B6 hosts (C57BL/6 J-Tyr^{cBrd})(Reid and Tessarollo, 2009). Line 1513 produced 90% chimeras and was used for subsequent electroporation of the *Fgf3*-targeting construct as previously described (Tessarollo et al., 2009). Clones were then picked and screened by Southern and SNP-assays described below. Clone 7033 was selected and injected into albino-B6 hosts (C57BL/6 J-Tyr^{cBrd})(Reid and Tessarollo, 2009). Mice displaying 90% chimerism were selected for breeding. The neomycin cassette was removed from the $Fgf4^{flox}$ locus through crossing to βActin-Flpe strain (Rodriguez et al., 2000). The $Fgf4^{\Delta}$ line was generated by crossing $Fgf4^{flox}$ mice to TCre (Perantoni et al., 2005), which has germline recombination activity. *Fgf3-Fgf4-cis* mice will be available to the research community upon acceptance of this manuscript.

SNP-assays for Determination of Cis vs Trans Targeting

To determine if targeted *Fgf3* and *Fgf4* alleles were in cis we took advantage of the hybrid 129/B6 nature of the ESCs. For the *Fgf4* targeted allele, we found a SNP within exon 2 of the B6 allele that created an *Nla*III/*Hin*1II site that was absent in the 129 allele. PCR primers flanking this site were designed such that insertion of the Neo cassette would disrupt amplification of the targeted allele (5′-CAGACTGAGGCTGGACTTGAGG and 5′-

GTGACCAACACACAAGTGTATGTGTGG). PCR amplification resulted in several nonspecific bands that were eliminated by cloning the PCR products in to TOPO2.1 (Thermofisher) and using this as template for subsequent PCR amplification. PCR digestion with *Nla*III or *Hin*1II yielded one uncut band in 129 (398 bp), two bands in B6 (268 bp and 130 bp), and two bands in the targeted clone 1513 (268 bp and 130 bp), thus indicating that the targeting event took place on the 129 allele (leaving the B6 allele available for PCR amplification). Sequencing these PCR products confirmed our analysis. A similar assay was designed for *Fgf3* in which a SNP was identified that created a *Hpy*AV site only within the B6 allele in a region that is deleted by insertion of the hygromycin selection cassette in our *Fgf3* targeting strategy. Primers were designed that flank the SNP (5′-CCACCCATGTACCATCCT-TACACC and 5′-CACCATCTCATGGTCCTTGTGGC). Following PCR amplification, digestion with *Hpy*AV yielded one uncut band in 129 (667 bp), two bands in B6 (266 bp and 401 bp), and two bands in the targeted clone 1513 (266 bp and 401 bp), thus indicating that the targeting event took place on the 129 allele, confirming cis-targeting to the $Fgf4^{flox}$ alleles.

Southern Blot

Digoxigenin labeled probes were made by PCR amplification using DIG DNA Labeling Mix (Roche 11277065910) from genomic DNA. Primers for *Fgf3* probe: 5′-CGAGCACTTACTTACTGAGCCATCC and 5′-CAGATCTATAGAGTGAAACAGCCAGGC. Primers for *Fgf4* probe: 5′-ACTGCAGGCTGAAAGGTGTC and 5′-TAAGTGCCTGGGAGAGATAGGATG. Non-radioactive Southern blots performed as described by manufacturer (Roche, DIG Application Manual for Filter Hybridization).

Genotyping

Targeted lines are maintained by assaying for the presence of hygromycin cassette found in $Fgf3^{\Delta}$ (5′-GCCATGTAGTGTATTGACCGATTCC and 5′-GCCTGACCTATTGCA-TCTCCCG) and/or presence of the *LoxP* site found in $Fgf4^{flox}$ (5′-CAGACTGAGGCTG-GACTTGAGG and 5′-CCTCTTGGGATCTCGATGCTGG). Homozygosity is determined by looking for the absence of the *Fgf3* wild type allele (5′-CTGCCTATGTGCTATAT-CCATGG and 5′-GGACGTATGAACGAGTGTATAGATGG) and/or loss of the wild type band in the $Fgf4^{flox}$ PCR. $Fgf4^{\Delta}$ was detected using the primers: (5′-CTCAGGAA-CTCTGAGGTAGATGGGG and 5′-ATCGGATTCCACCTGCAGGTGC). TCre was detected as previously described (Perantoni et al., 2005).

mRNA Whole Mount in situ hybridization and Skeletal Preparations

mRNA whole mount in situ hybridization was performed as previously described (Naiche et al., 2011). Skeletal preparations were performed as previously described (Nagy, 2003).

Measurements and Statistics

Measurements were performed in Photoshop using the ruler tool on images taken at the same magnification and resolution. All error bars represent SEM, t-test used to determine significance assuming unequal variances.

Acknowledgments

We would like to thank T. Schimmang for providing DNA used to construct the *Fgf3-targeting* construct. We are grateful to C. Elder and E. Truffer for technical assistance. This work was supported by the Center for Cancer Research of the Intramural Research Program of the National Institutes of Health through the National Cancer Institute.

References

Alvarez Y, Alonso MT, Vendrell V, Zelarayan LC, Chamero P, Theil T, Bosl MR, Kato S, Maconochie M, Riethmacher D, Schimmang T. 2003; Requirements for FGF3 and FGF10 during inner ear formation. Development. 130:6329–6338. [PubMed: 14623822]

Boulet AM, Capecchi MR. 2012; Signaling by FGF4 and FGF8 is required for axial elongation of the mouse embryo. Dev Biol. 371:235–245. [PubMed: 22954964]

Boulet AM, Moon AM, Arenkiel BR, Capecchi MR. 2004; The roles of Fgf4 and Fgf8 in limb bud initiation and outgrowth. Dev Biol. 273:361–372. [PubMed: 15328019]

Feldman B, Poueymirou W, Papaioannou VE, DeChiara TM, Goldfarb M. 1995; Requirement of FGF-4 for postimplantation mouse development. Science. 267:246–249. [PubMed: 7809630]

Goetz R, Mohammadi M. 2013; Exploring mechanisms of FGF signalling through the lens of structural biology. Nat Rev Mol Cell Biol. 14:166–180. [PubMed: 23403721]

Goldfarb M. 2005; Fibroblast growth factor homologous factors: evolution, structure, and function. Cytokine Growth Factor Rev. 16:215–220. [PubMed: 15863036]

Gomez C, Ozbudak EM, Wunderlich J, Baumann D, Lewis J, Pourquie O. 2008; Control of segment number in vertebrate embryos. Nature. 454:335–339. [PubMed: 18563087]

Hatch EP, Noyes CA, Wang X, Wright TJ, Mansour SL. 2007; Fgf3 is required for dorsal patterning and morphogenesis of the inner ear epithelium. Development. 134:3615–3625. [PubMed: 17855431]

Itoh N. 2010; Hormone-like (endocrine) Fgfs: their evolutionary history and roles in development, metabolism, and disease. Cell Tissue Res. 342:1–11. [PubMed: 20730630]

Jackson A, Kasah S, Mansour SL, Morrow B, Basson MA. 2014; Endoderm-specific deletion of Tbx1 reveals an FGF-independent role for Tbx1 in pharyngeal apparatus morphogenesis. Dev Dyn. 243:1143–1151. [PubMed: 24812002]

Li CY, Prochazka J, Goodwin AF, Klein OD. 2014; Fibroblast growth factor signaling in mammalian tooth development. Odontology. 102:1–13. [PubMed: 24343791]

Long YC, Kharitonenkov A. 2011; Hormone-like fibroblast growth factors and metabolic regulation. Biochim Biophys Acta. 1812:791–795. [PubMed: 21504790]

Mansour SL, Goddard JM, Capecchi MR. 1993; Mice homozygous for a targeted disruption of the proto-oncogene int-2 have developmental defects in the tail and inner ear. Development. 117:13–28. [PubMed: 8223243]

Mansour SL, Thomas KR, Capecchi MR. 1988; Disruption of the proto-oncogene int-2 in mouse embryo-derived stem cells: a general strategy for targeting mutations to non-selectable genes. Nature. 336:348–352. [PubMed: 3194019]

Mansouri A, Voss AK, Thomas T, Yokota Y, Gruss P. 2000; Uncx4.1 is required for the formation of the pedicles and proximal ribs and acts upstream of Pax9. Development. 127:2251–2258. [PubMed: 10804168]

Miyagawa S, Moon A, Haraguchi R, Inoue C, Harada M, Nakahara C, Suzuki K, Matsumaru D, Kaneko T, Matsuo I, Yang L, Taketo MM, Iguchi T, Evans SM, Yamada G. 2009; Dosage-dependent hedgehog signals integrated with Wnt/beta-catenin signaling regulate external genitalia formation as an appendicular program. Development. 136:3969–3978. [PubMed: 19906864]

Moon AM, Boulet AM, Capecchi MR. 2000; Normal limb development in conditional mutants of Fgf4. Development. 127:989–996. [PubMed: 10662638]

Nagy, A, Gertsenstein, M, Vintersten, K, Behringer, R. Manipulating the Mouse Embryo. Cold Spring Harbor Laboratory Press; Cold Spring Harbor, NY: 2003.

Naiche LA, Holder N, Lewandoski M. 2011; FGF4 and FGF8 comprise the wavefront activity that controls somitogenesis. Proc Natl Acad Sci U S A. 108:4018–4023. [PubMed: 21368122]

Niswander L, Martin GR. 1992; Fgf-4 expression during gastrulation, myogenesis, limb and tooth development in the mouse. Development. 114:755–768. [PubMed: 1618140]

Olsen SK, Garbi M, Zampieri N, Eliseenkova AV, Ornitz DM, Goldfarb M, Mohammadi M. 2003; Fibroblast growth factor (FGF) homologous factors share structural but not functional homology with FGFs. J Biol Chem. 278:34226–34236. [PubMed: 12815063]

Ornitz DM, Itoh N. 2015; The Fibroblast Growth Factor signaling pathway. Wiley Interdiscip Rev Dev Biol. 4:215–266. [PubMed: 25772309]

Perantoni AO, Timofeeva O, Naillat F, Richman C, Pajni-Underwood S, Wilson C, Vainio S, Dove LF, Lewandoski M. 2005; Inactivation of FGF8 in early mesoderm reveals an essential role in kidney development. Development. 132:3859–3871. [PubMed: 16049111]

Reid SW, Tessarollo L. 2009; Isolation, microinjection and transfer of mouse blastocysts. Methods Mol Biol. 530:269–285. [PubMed: 19266343]

Rodriguez CI, Buchholz F, Galloway J, Sequerra R, Kasper J, Ayala R, Stewart AF, Dymecki SM. 2000; High-efficiency deleter mice show that FLPe is an alternative to Cre-loxP. Nat Genet. 25:139–140. [PubMed: 10835623]

Sun C, Bernards R. 2014; Feedback and redundancy in receptor tyrosine kinase signaling: relevance to cancer therapies. Trends Biochem Sci. 39:465–474. [PubMed: 25239057]

Sun X, Lewandoski M, Meyers EN, Liu YH, Maxson RE Jr, Martin GR. 2000; Conditional inactivation of Fgf4 reveals complexity of signalling during limb bud development. Nat Genet. 25:83–86. [PubMed: 10802662]

Sun X, Mariani FV, Martin GR. 2002; Functions of FGF signalling from the apical ectodermal ridge in limb development. Nature. 418:501–508. [PubMed: 12152071]

Tessarollo L, Palko ME, Akagi K, Coppola V. 2009; Gene targeting in mouse embryonic stem cells. Methods Mol Biol. 530:141–164. [PubMed: 19266325]

Urness LD, Bleyl SB, Wright TJ, Moon AM, Mansour SL. 2011; Redundant and dosage sensitive requirements for Fgf3 and Fgf10 in cardiovascular development. Dev Biol. 356:383–397. [PubMed: 21664901]

Wright TJ, Hatch EP, Karabagli H, Karabagli P, Schoenwolf GC, Mansour SL. 2003; Expression of mouse fibroblast growth factor and fibroblast growth factor receptor genes during early inner ear development. Dev Dyn. 228:267–272. [PubMed: 14517998]

Yang H, Wang H, Jaenisch R. 2014; Generating genetically modified mice using CRISPR/Cas-mediated genome engineering. Nature protocols. 9:1956–1968. [PubMed: 25058643]

Yoon JK, Wold B. 2000; The bHLH regulator pMesogenin1 is required for maturation and segmentation of paraxial mesoderm. Genes Dev. 14:3204–3214. [PubMed: 11124811]

You Y, Bersgtram R, Klemm M, Nelson H, Jaenisch R, Schimenti J. 1998; Utility of C57BL/6J x 129/SvJae embryonic stem cells for generating chromosomal deletions: tolerance to gamma radiation and microsatellite polymorphism. Mamm Genome. 9:232–234. [PubMed: 9501308]

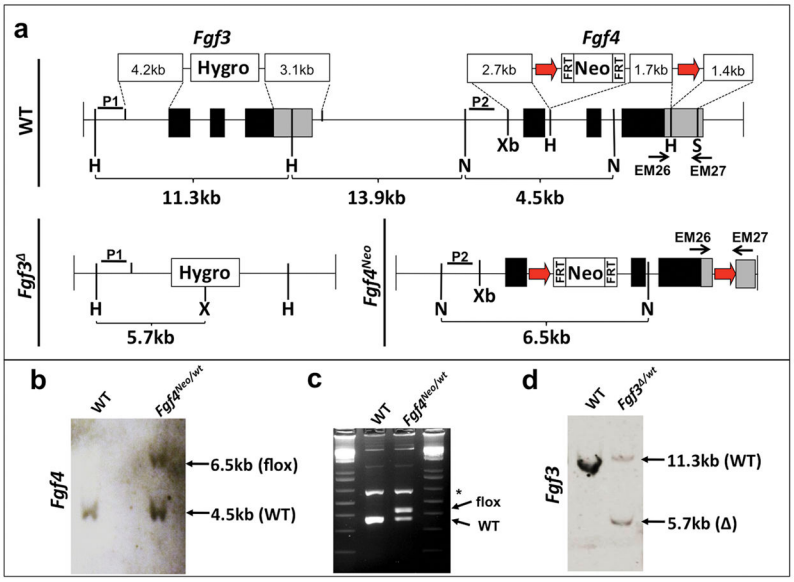

FIG. 1.

Targeting of the *Fgf3* and *Fgf4* loci. **(a)** (Top) Diagram of a portion of chromosome 7 showing close proximity of *Fgf3* and *Fgf4* with targeting vectors indicated above the respective wild type (WT) gene. (Bottom, left) Resulting targeted allele for *Fgf3* (*Fgf3*$^{\Delta}$) in which the *Fgf3* coding region was replaced with a hygromycin resistance cassette. (Bottom, right) Resulting targeted allele *Fgf4* (*Fgf4*^{Neo}) in which Exons 2 and 3 of *Fgf4* were flanked with LoxP sites and a neomycin resistance cassette was inserted into the first intron. **Red arrows** represent LoxP sites, brackets indicate distances between select restriction sites: *Hind*III (H), *Nhe*I (N), *Xba*I (Xb), *Sal*I (S), *Xho*I (X). Relative position of probes used for Southern blot analysis for *Fgf3* (P1) and *Fgf4* (P2) indicated by **black lines**. Position of primers used for detection of 3′ LoxP site indicated by arrows, EM26 and EM27. Black bars indicate translated exonic regions, gray bars indicate 3′ untranslated regions. **(b)** Representative autoradiogram for southern blot analysis of the targeted *Fgf4* allele, with DNA digested with *Nhe*I. As shown in **a**, the wild type *Fgf4* locus contains a pair of *Nhe*I sites spaced 4.5kb apart (WT band in **b**). Also shown in **a**, insertion the LoxP site and FRT-flanked neomycin resistance cassette increases the size of the *Nhe*I digestion product by 2kb (flox band in **b**). **(c)** PCR was performed on DNA from ES-cell lysates to confirm the presence of the 3′ LoxP site; non-specific band produced by PCR amplification denoted with **asterisk. (d)** Representative autoradiogram of Southern blot analysis for the targeted *Fgf3* allele, DNA is digested with *Hind*III and *Xho*I. As shown in **a**, the wild type *Fgf3* locus contains a pair of *Hind*III sites spaced 11.3kb apart, but lacks an *Xho*I site (WT band in **d**). As shown in **a**, replacement of the *Fgf3* coding region with the hygromycin resistance cassette introduces an *Xho*I site. Following digestion of targeted genomic DNA with *Hind*III and *Xho*I, a 5.7kb band is detected (Δ band in **d**).

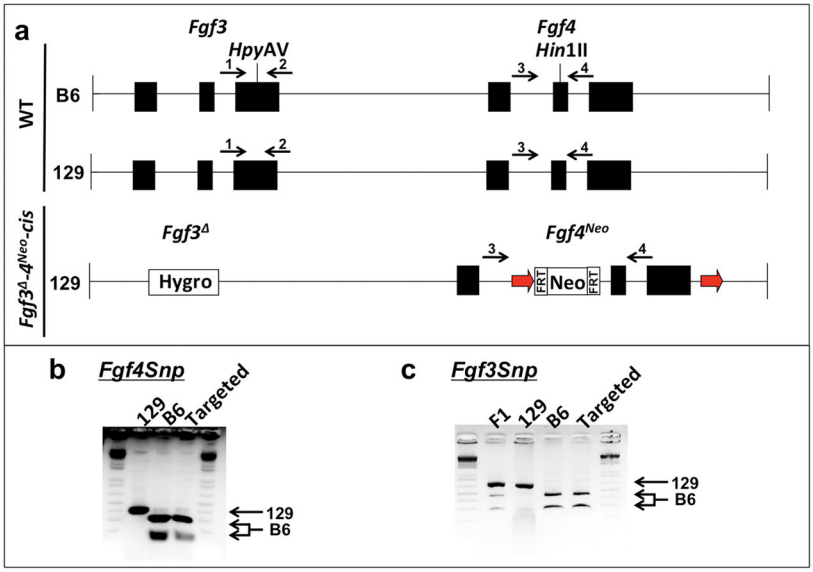

FIG. 2.

Determination of cis targeting of *Fgf3* and *Fgf4*. **(a)** Diagram of WT *Fgf3* and *Fgf4* loci on B6 or 129 chromosome. The B6 chromosome contains an *Fgf3* allele with a SNP within exon 3 that creates an *Hpy*AV restriction site and *Fgf4* allele with a SNP within exon 2 that creates a *Hin*1II restriction site. PCR assays were designed across these regions so that these sites, if present, were unique within the amplicon. Replacement of *Fgf3* coding regions with the hygromycin resistance cassette or insertion of the Frt-flanked neomycin cassette in *Fgf4* disrupted amplification of the targeted alleles (*Fgf3Snp* primers: 1 and 2; *Fgf4Snp* primers: 3 and 4). **(b)** Representative DNA gel electrophoresis showing *Fgf4Snp* PCR products following digestion with *Hin1*II. Digestion of PCR products amplified from control 129 tail DNA yielded a full-length 398 bp band and digestion of PCR products amplified from control B6 tail DNA resulted in 268 bp and 130 bp bands. Digestion of the amplicon from the targeted clone yielded a pair of bands corresponding to a remaining untargeted B6 allele; hence we had targeted the 129 chromosome. **(c)** Representative DNA gel electrophoresis showing *Fgf3Snp* PCR products following digestion with *Hpy*AV. Digestion of PCR products amplified from the parental F1 ES cells (B6/129), yielded a full-length 667 bp band (corresponding to amplified 129 allele), and 266 bp and 401 bp bands (corresponding to amplified B6 allele); digestion of amplicons generated from 129 or B6 tail DNA yielded single 667 bp or a pair of 266 bp and 401 bp bands, respectively. Digestion of the amplicon from the targeted clone yielded a pair of bands corresponding to a remaining untargeted B6 allele, thus confirming cis targeting of $Fgf3^{\Delta}$ and $Fgf4^{Neo}$ to the 129 allele.

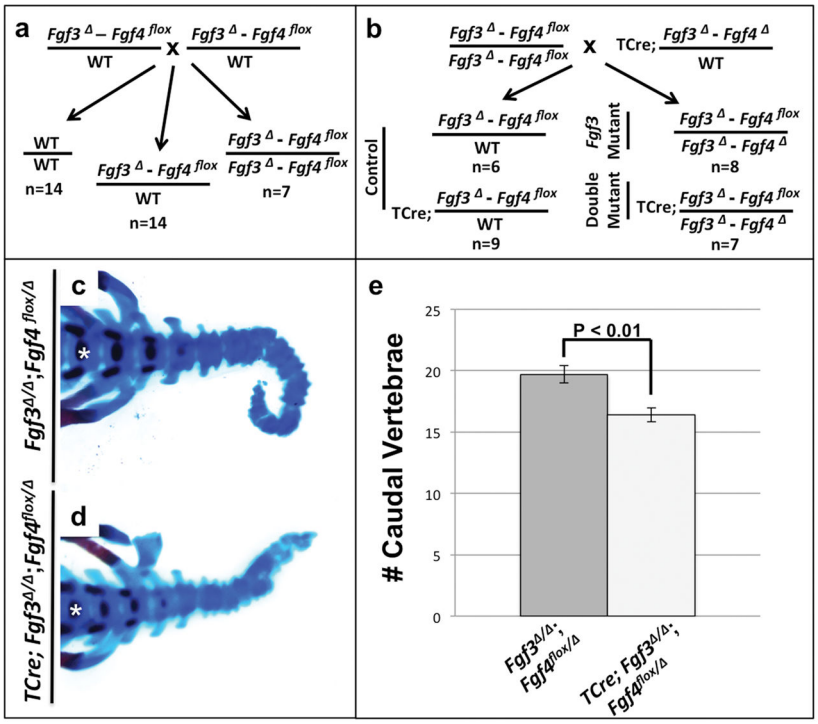

FIG. 3.

Fgf3 and *Fgf4* act redundantly in caudal axis extension. **(a)** Genetic cross to generate $Fgf3^{\Delta/\Delta};Fgf4^{flox/flox}$ and resultant progeny with observed numbers at E18.5. **(b)** Experimental cross with observed numbers of progeny at E18.5. **(c, d)** Skeletal preparations of E18.5 $Fgf3^{\Delta/\Delta};Fgf4^{flox/\Delta}$ (n=13) and TCre;$Fgf3^{\Delta/\Delta};Fgf4^{flox/\Delta}$ (n=8) mutants; the first caudal vertebra in each sample is labeled with an asterisk. **(c)** Total caudal vertebrae number; p-value determined by T-test, error bars represent SEM.

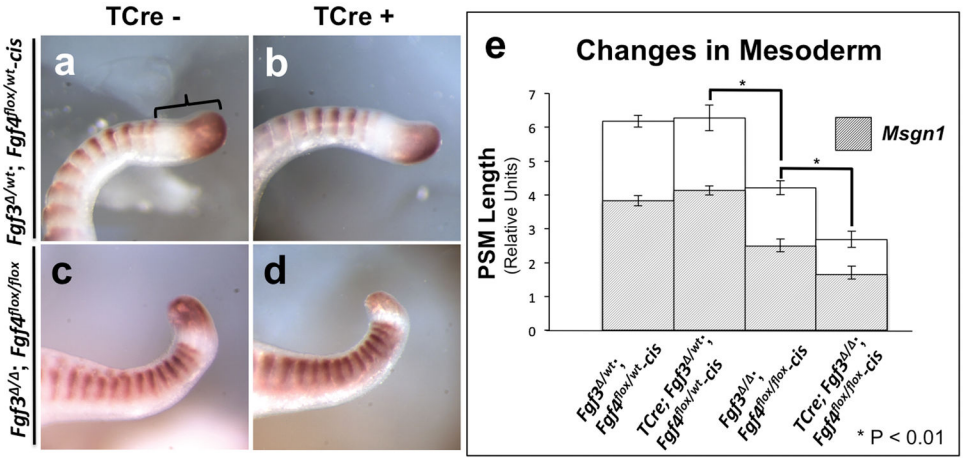

FIG. 4.

Fgf3 and *Fgf4* are redundant in tailbud maintenance. **(a–d)** *Uncx4.*1 (somite) and *Msgn1* (PSM) mRNA expression in E10.5 (38–40 somite stage) control $Fgf3^{\Delta/wt}$;$Fgf4^{flox/wt}$ (n=9)or TCre;$Fgf3^{\Delta/wt}$;$Fgf4^{flox/wt}$ (n=3), $Fgf3^{\Delta/\Delta}$;$Fgf4^{flox/\Delta}$ (n=7) or *TCre;Fgf3;Fgf4* (n=5) embryos; **bracket** in **a** shows measurement taken for total PSM in **e. (e)** Measurement of total PSM anterior-posterior length (**white bar**) or *Msgn1* domain (**hashed bar**) for each genotype; p-value determined by T-test, error bars represent SEM.